Development of a 5G-Optimized MIMO Antenna with Enhanced Isolation Using Neutralization Line and SRRs Metamaterials

Chaker Essid[1], Linda Chouikhi[2], Alsharef Mohammad[3], Bassem Ben Salah[4], Hedi Sakli[5]*
SERCOM Laboratory-Tunisia Polytechnic School, University of Carthage, La Marsa 2078, Tunisia[1, 2, 4]
Department of Electrical Engineering-College of Engineering, Taif University, Taif, Saudi Arabia[3]
EITA Consulting, 7 Rue du Chant des oiseaux, 78360 Montesson, France[3, 5]
MACS Research Laboratory RL16ES22-National Engineering School of Gabes, Gabes University, Gabes, 6029, Tunisia[4, 5]

***Abstract*—This paper presents the design of a Multiple Input Multiple Output (MIMO) antenna intended for 5G wireless applications operating in the 3.5 GHz frequency range. The MIMO system consists of two adjacent antennas, measuring 100 mm × 80 mm × 1.6 mm, with spacing between radiating elements equal to one-eighth of the wavelength (λ/8). The antenna is constructed on an FR4 substrate with a permittivity of 4.3, and a microstrip line is employed for feeding the patch. Several techniques are employed to enhance the isolation between the antennas. Specifically, two decoupling methods are explored: the use of a neutralization line (NL) and the incorporation of metamaterial split-ring resonators (SRRs). Simulation results demonstrate substantial isolation, exceeding 20 dB with SRR implementation and more than 23 dB with the NL approach. Both individual antennas and the MIMO configuration are simulated, analyzed, and then physically fabricated for measurement, exhibiting good agreement between measured and simulated results. The study investigates the impact of each technique on antenna to determine the optimal configuration for the applications of 5G and IOT in different fields such as health (wireless medical telemetry systems (WMTS)). Remarkably, the introduction of metamaterial (MTM) with SRRs achieves a noteworthy reduction of mutual coupling by 23 dB while minimizing the mutual coupling to about 23 dB with NL insertion.**

***Keywords*—5G; antenna; MIMO; SRRs metamaterials; isolation; IOT; neutralization line (NL)**

I. INTRODUCTION

The increasing requirement for significantly improved data rates and extensive capacity has fueled the continuous evolution of technology and the progression of mobile and wireless communication networks. This necessity has led to the emergence of a new phase in mobile communication, known as the fifth generation or 5G [1]. 5G cellular networks are considered a critical component in enabling the next generation of the Internet, commonly known as the Internet of Things (IoT) [2, 3]. IoT essentially involves connecting a wide range of devices and people to a central IoT platform [4]. The core concept of IoT revolves around using sensors to collect data, which is then sent to a server for analysis. This analysis generates insights that are transformed into actions, leading to the creation of intelligent environments such as smart homes and vehicles [5]. The evolution of IoT enables the connection of numerous devices to the internet, with predictions suggesting that over 28 billion smart devices will be connected worldwide by 2021 [6]. Moreover, machine-to-machine (M2M) communication is expected to be utilized in over 15 billion devices, emphasizing the magnitude of IoT's impact. However, it is crucial to acknowledge that most of these connected devices depend on batteries for power, presenting environmental challenges due to their polluting nature [7].

To address this concern, researchers at the Georgia Institute of Technology in the United States have developed a rectifying antenna, often called a Rectenna [8]. The Rectenna integrates a rectifier and an antenna, acting as a vital element in wireless telecommunications systems. Its distinctive ability is to convert 5G waves into electric current, which could eventually enable mobile operators to serve as power providers for IoT devices [9, 10]. With the introduction of 5G, mobile operators are tasked with deploying 5G base stations in the 3.4-3.6 GHz band, using a specific operational mode called Time Division Multiplexing (TDD) [11]. TDD involves dividing the frequency band into separate transmit and receive segments, allowing the same frequency band to be used for both transmission directions. This feature is particularly beneficial for Massive Multiple Input Multiple Output (MIMO) technology [12], which has gained traction in wireless communication systems, especially in the context of 5G applications.

The antennas operating at 3.5 GHz are used in wireless medical telemetry systems (WMTS) to monitor patients' vital signs and transmit this data wirelessly to medical personnel [13]. These antennas enable the transmission of medical data over short to medium distances in various healthcare settings, providing reliable and high-speed communication for real-time monitoring and prompt responses to emergency situations [14,15].

However, the increasing number of antennas on a limited-size electrical component can lead to a phenomenon called mutual coupling (MC) [15, 16]. MC occurs when current densities generated by nearby antennas alter the radiation characteristics of neighboring antennas, potentially degrading MIMO system performance [17,18]. Although various techniques, including metamaterials (MTM) [19-21],

neutralization lines (NL) [22, 23], Defected Ground Structure (DGS) [24], parasitic or slot elements [25], have been explored to mitigate MC, there is ongoing research to enhance the isolation characteristics of MIMO antennas.

A variety of research has been done to increase the isolation characteristics of MIMO antennas by inserting MTM cells. The authors in [19] propose a flag-shaped MIMO antenna using MTM technique in the frequency of Sub-6 GHz 5G applications. It consists of two antennas printed on the FR-4 substrate and separated by a distance of λ/2. Results show a low mutual coupling reduction of 16dB, and the gain obtained was 3.28 dB at 3.1 GHz. Research in [20] applies the same technique to increase the decoupling over the two MIMO antennas spaced 2 mm. This method provides a coupling of minus of −45 dB in the 4.8 - 5 GHz band to be a suitable candidate for 5G applications.

Another idea developed by the researcher in [21], it is based on placing a MTM isolating structure between two circular antenna patches. After insertion of this cell MTM, it provides -23 dB of mutual coupling reduction between the two radiator elements. Other types of metamaterials are used to increase the decoupling between antennas, such as Electromagnetic Band Gap (EBG) [22], and Frequency Selective Surface (FSS) [23].

An alternative approach to enhance the performance of MIMO systems is introduced in [22], which involves the incorporation of a neutralization line between four L-monopole antennas with a semi-elliptical radiating patch. This method achieves a coupling reduction of approximately 20 dB between the elements of the antenna array within the frequency range of 3.36 - 3.68 GHz. Essentially, this line is modeled as an inductance to impede mutual coupling, functioning as a rejection filter. Similarly, a neutralization line is employed between two elliptical multi-antennas around the resonant frequency of 3.5 GHz for 5G mobile applications [24]. This configuration results in a transmission magnitude of less than −24 dB at the operating frequency, thereby improving gain, diversity, and radiation efficiency. Other researchers have adopted this isolation technique in [25], which consists of two tri-band antenna elements separated by 0.03 λ0. These two antennas are connected by U-shaped and inverted U-shaped NLs, suppressing the MC about −15 dB, −30 dB, and −20 dB at 2.3 GHz, 3.5 GHz, and 5.7 GHz, respectively.

The band 3.5 GHz (3.4 - 3.8) GHz has been exclusively allocated to the 5G mobile network, serving as the "heart" of 5G and providing subscribers with a high quality of service. Among the various frequencies utilized by 5G (700 MHz, 3.5 GHz, and 26 GHz), this band is considered sufficient as it offers adequate coverage and capacity [25]. The primary objective of this research is to evaluate the performance of MIMO antennas employing various techniques, with a focus on minimizing mutual coupling. Given that placing antennas in close proximity can lead to MC, the literature has explored methods for reducing MC, with an emphasis on isolation techniques involving NL and metamaterials. This paper also provides insights into the magnetic phenomena underpinning these methods and emphasizes the importance of parametric studies to optimize simulation results.

However, the deployment of 5G networks and IoT devices faces several challenges, including mutual coupling in Multiple Input Multiple Output (MIMO) antennas, which can degrade system performance. Addressing these challenges is crucial for realizing the full potential of 5G and IoT. This research is motivated by the need to enhance the isolation characteristics of MIMO antennas, thereby improving the overall performance and reliability of 5G networks and IoT applications. By developing novel techniques to reduce mutual coupling, we aim to contribute to the advancement of wireless communication systems and enable more efficient and reliable connectivity for a wide range of applications.

The main contributions of this paper are the development and evaluation of two innovative techniques for enhancing the isolation characteristics of Multiple Input Multiple Output (MIMO) antennas operating in the 3.5 GHz frequency band, which is crucial for 5G applications. Firstly, we propose the use of a neutralization line (NL) to significantly reduce mutual coupling between adjacent antennas, achieving an isolation of over 23 dB. Secondly, we introduce the integration of metamaterial split-ring resonators (SRRs) to further minimize mutual coupling, resulting in an isolation improvement of approximately 23 dB. These techniques are thoroughly analyzed through simulations and validated through physical measurements, demonstrating their effectiveness in real-world scenarios. The implications of these contributions are substantial for 5G and IoT applications. By improving the isolation characteristics of MIMO antennas, we can enhance the overall performance and reliability of 5G networks, enabling higher data rates, reduced interference, and better coverage. This is particularly beneficial for IoT applications, where reliable and high-speed communication is essential for real-time monitoring and control of various devices and systems. Our findings provide valuable insights and practical solutions for the design of advanced MIMO antennas, contributing to the advancement of wireless communication technologies and the realization of the full potential of 5G and IoT.

The structure of the paper is as follows: Section II elaborates on the design of the proposed antenna. Subsequently, Section III presents the simulation results of the MIMO antenna system. Section IV delves into the characteristics of the MIMO system incorporating decoupling techniques. Lastly, the conclusions are summarized in the final section.

II. Design of New Patch Antenna

To ensure the optimal performance of our advanced multi-antenna system, it is imperative to begin with a comprehensive understanding of the fundamental principles of antenna design. In our proposed project, our focus has been centered on three critical aspects: the antenna's geometric configuration, the designated frequency range for operation, and the implementation of techniques to minimize MC within the multi-antenna system.

Our initial step entailed the design of a rectangular patch antenna, which was powered through a microstrip transmission line with a specific width denoted as wf, adhering to the requisite 50-ohm characteristic impedance for the transmission line. The radiating element, characterized by dimensions Lp × Wp, was physically fabricated on an FR-4 substrate, with dimensions L × W, and a specified thickness (h). The substrate was chosen for its cost-effectiveness and the expeditious prototyping capabilities it offers. The resonant frequency was set at 3.5 GHz, a choice determined through calculations employing equations outlined in [26].

A pivotal step in enhancing the antenna's performance was the strategic alteration of its structure, which involved the incorporation of cuts and slots in both the radiating element and the ground plane (show Fig. 1). Fig. 2 illustrates the results of simulation of these structural adjustments in terms of the reflection coefficient (S11).

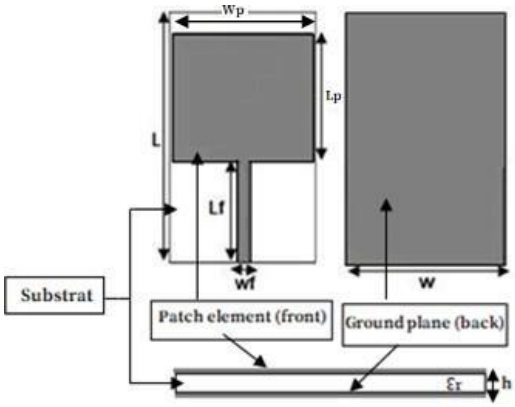

Fig. 1. Structure of the basic antenna in front and back views.

Remarkably, the implementation of partial modifications to the ground plane, featuring two small square patches on the left and right, yielded a maximum S11 value of approximately -20 dB within the 3.4 - 3.8 GHz operational band. To further broaden the bandwidth and ensure that the signal reflection remained below -10 dB, we introduced two triangular cuts at the top of the radiating element. This modification extended the frequency band from 2.2 GHz to 4.5 GHz. The incorporation of two additional triangular cuts at the bottom of the patch resulted in a notable enhancement in the antenna's adaptation to the 3.5 GHz frequency, with an S11 value now falling below -59 dB.

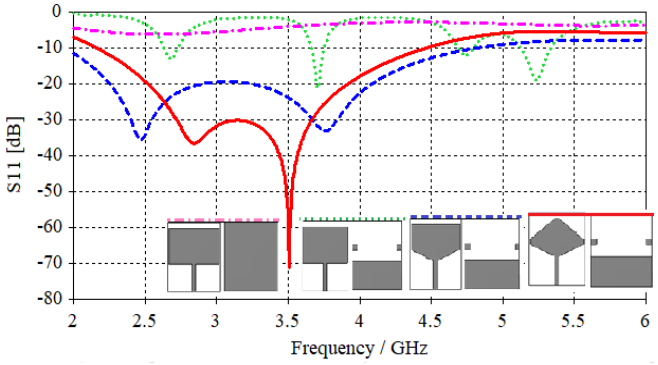

Fig. 2. Reflection coefficient S11 of the proposed antenna with and without modifications and optimized final antenna.

In order to enhance the performance of our antenna, the first crucial step involves modifying the structure by incorporating cuts and slots in the radiating element and the ground plane. The reflection coefficient (S11) results for all configurations are illustrated in Fig. 2. By making the ground plane partial, a maximum S11 value of approximately -20 dB in the 3.4-3.8 GHz operating band is achieved. To further extend the bandwidth (ensure a signal below -10 dB), two triangular cuts are applied at the top of the radiating element, resulting in a band spanning from 2.2 GHz to 4.5 GHz (as shown in Fig. 3).

Fig. 3 indicates that the optimum position is L4 = 8 mm, which provides the highest S11 at 3.5 GHz. By introducing two additional triangular cuts at the bottom of the patch, we fixed the optimal value of L4 at 8 mm and varied the values of L3 (ranging from 10 to 16 mm).

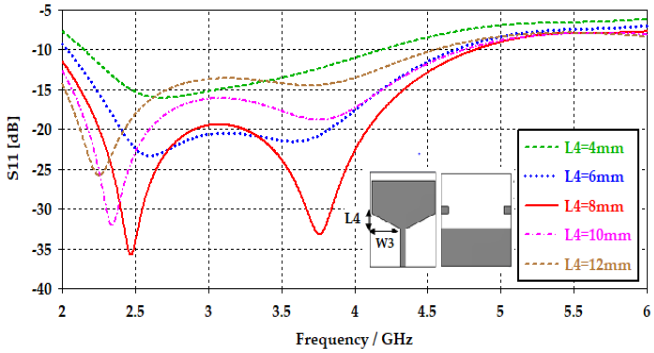

Fig. 3. Reflexion coefficient of the proposed antenna with different values of L4.

As illustrated in Fig. 4, the adaptation to the 3.5 GHz frequency shows improvement for L3=14 mm compared to the previous results, with S11 below -59 dB.

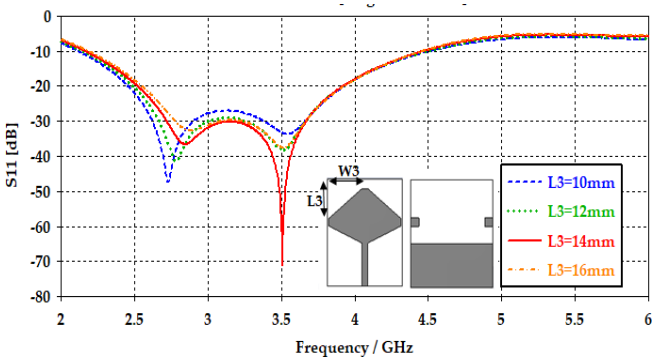

Fig. 4. Reflexion coefficient of the proposed antenna with different values L3.

The selections made for the dimensions presented in Table I were made with precision, considering both impedance matching and the constraints related to system size, all while considering the specific applications for which the antenna is intended. The incorporation of a slotted ground within the proposed antenna serves the purpose of enhancing the antenna's performance by amplifying inter-element isolation and reducing overall reflection (see Fig. 5).

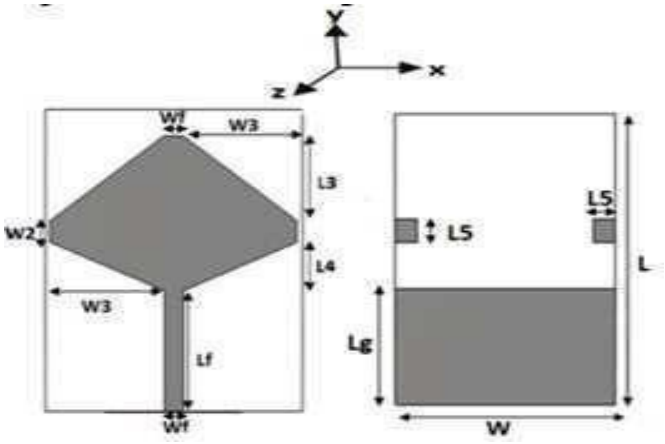

Fig. 5. Proposed antenna in front and bottom views.

TABLE I. OPTIMIZED DIMENSIONS OF THE PROPOSED ANTENNA

Components	Parameters	Values (mm)
Patch	Lf	20
	Wf	3.1
	W2	3.6
	W3	18.5
	L3	14
	L4	8
Dielectric substrate	W	40
	L	50
	h	1.6
	εr	4.4
Ground Plan	Lg	20
	L5	5

Fig. 6 presents the real and imaginary parts of the antenna impedance, revealing that at 3.5 GHz, the real part is approximately 50 Ω and the imaginary part is nearly 0 Ω. Consequently, the impedance demonstrates good adaptability. The antenna gain as a function of frequency is displayed in Fig. 7 within the [3.4-3.8] GHz band. It is observed that the maximum gain value obtained is around 2.8 dB at 3.5 GHz.

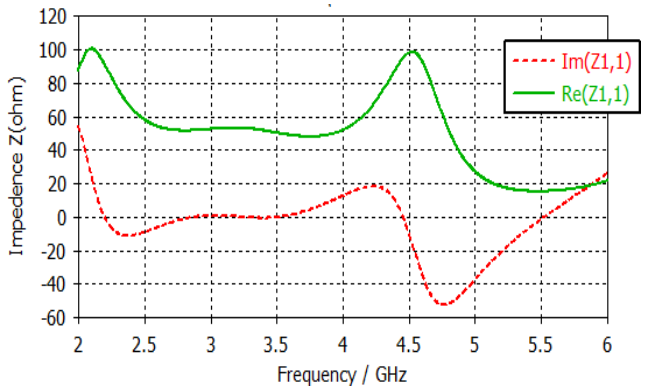

Fig. 6. Input impedance of the studied antenna.

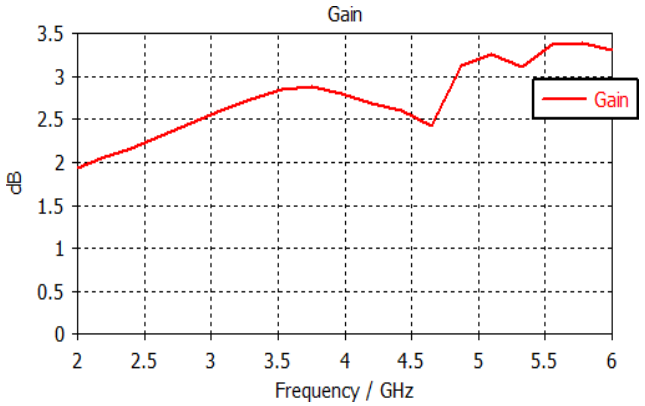

Fig. 7. Variation of gain as a function of frequency.

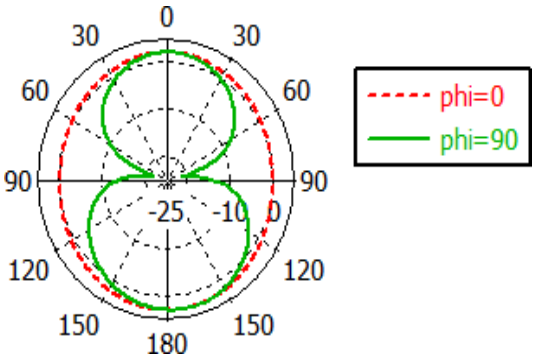

Fig. 8. Antenna radiation pattern at 3.5 GHz in E and H planes.

In Fig. 8, the radiation patterns of the proposed antenna are illustrated in the E and H planes (YZ plane with φ= 90° and XZ plane with φ= 0°, respectively) at 3.5 GHz. The antenna exhibits a unidirectional radiation pattern, which remains relatively consistent throughout the entire band.

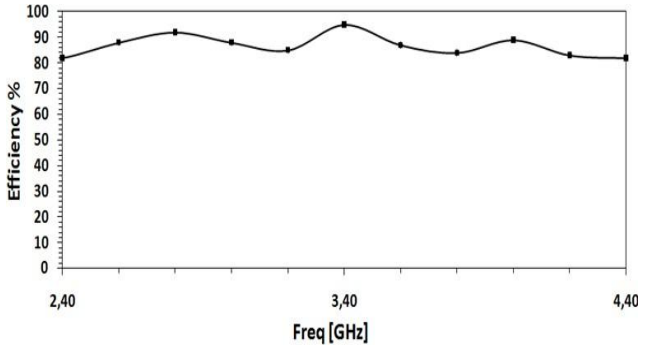

Fig. 9. Efficiency of the studied antenna versus frequency.

Fig. 9 provides compelling evidence of the exceptional efficiency of the antenna design we have put forth. Within the operational band, the efficiency of this antenna consistently surpasses the remarkable threshold of 80%. This is a noteworthy achievement, signifying the antenna's ability to effectively convert a substantial portion of the input power into radiated energy, thus enhancing its performance and applicability across a wide range of scenarios and applications. Fig. 10 shows the realized prototype of our antenna which is dedicated for many applications with an isolation necessarily exceeding 15 dB.

Fig. 10. Prototype of the proposed antenna.

The comparison between the simulation and the measured simulation results of S11 is thoughtfully displayed in Fig. 11. This comprehensive illustration underscores the integrity of our research, revealing a compelling alignment between the simulated data and the actual measurements across various frequencies within the operating band. This robust congruence between simulation results and real-world performance, particularly in the context of S11, stands as a testament to the accuracy and reliability of our antenna analysis. It signifies that our findings and the practical implementation of our antenna consistently correspond, instilling confidence in the veracity of our results and reinforcing the practical utility of the studied antenna design across a broad spectrum of frequencies within the operational range.

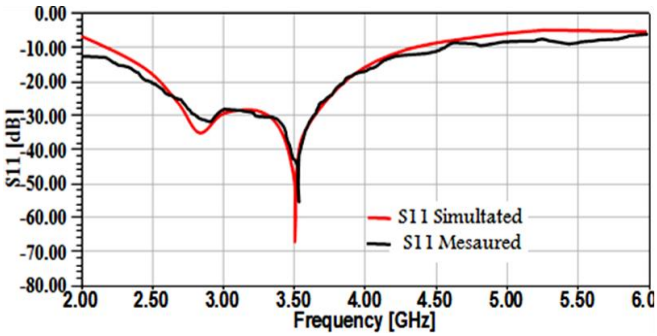

Fig. 11. Measured and simulated of S11 of the studied antenna versus frequency.

III. Study of Characteristics of the System MIMO

In this part, two techniques will be applied to two different antenna systems and each system consists of two antennas of the same configuration and size with left and right edges symmetrically. The first technique is based on the insertion of a neutralization line (NL) to reduce mutual coupling. The second technique is based on the integration of metamaterial, composed of a periodic structure consisting of three spring ring resonator (SRR) cells which are well detailed in the following section.

All measurements were conducted in an anechoic chamber, as shown in Fig. 12. The structure of the MIMO system before the application of the isolation methods is depicted in Fig. 13. The gap distance between the two-end edges of the two antennas is represented by 'e' and is optimized to 51 mm. An additional substrate of length 'a' equal to 11 mm is also introduced.

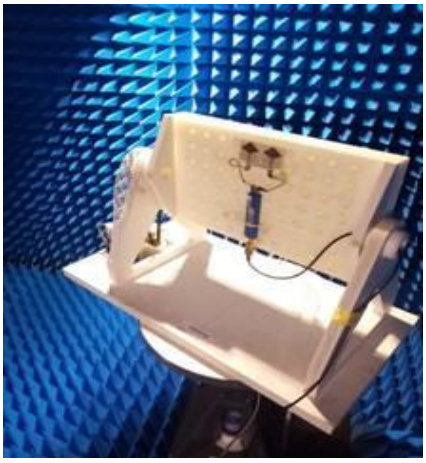

Fig. 12. Apparatus used to measure the antenna in the anechoic chamber.

The separation distance between the two edges of the antennas, represented by 'e', is set to e = λ/8 (where λ is the free space wavelength at the center frequency of 3.5 GHz). The overall size of the studied MIMO antenna system, comprising both substrates, is 100 mm × 80 mm × 1.6 mm, resulting in enhanced performance at 3.5 GHz.

The mutual coupling coefficients S21 and the simulated reflection coefficients S11 for various values of e (from 12.6 to 22.6 mm) are obtained and presented in Fig. 14 and 15, respectively. As shown in Fig. 12, we note that the impact on the S11 is relatively limited with unchanged bandwidth. From Fig. 13, we can see that the weakest coupling S21 is achieved with the smallest value of d (from 12.6 to 22.6 mm). The lowest coupling is obtained with the smallest value of e (e is 12.6 mm) and to maintain the antenna quality and the overall size of the MIMO antenna. MIMO antennas must be independent with minimal coupling to work well. So, to reduce the space between them, an efficient approach is to work on the space between them.

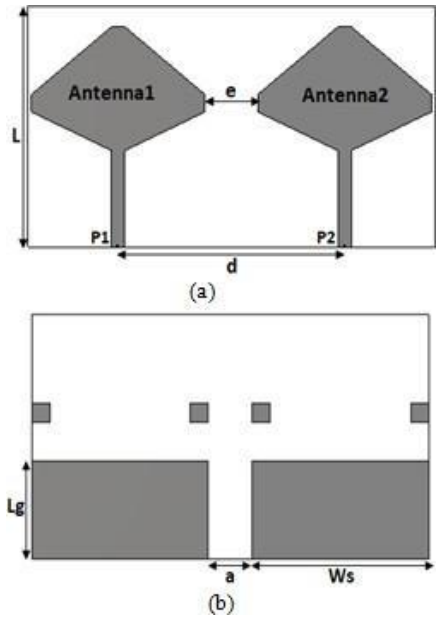

Fig. 13. Structure of the system MIMO antenna: (a) front view, (b) back view.

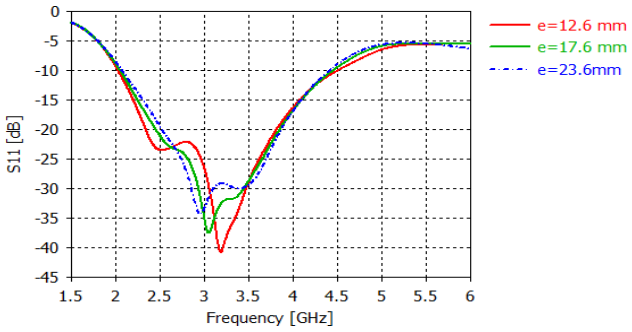

Fig. 14. Reflection Coefficient S_{11} of the suggested antenna at various e values.

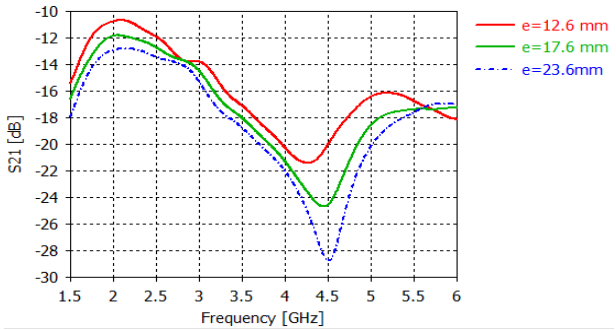

Fig. 15. Transmission coefficient S21 of the proposed antenna in different values of e.

Fig. 16 presents the realized prototype of the two symmetric antennas. The measured reflection (S11) and transmission (S21) parameters are displayed in Fig. 17 and 18, respectively. These figures provide a comparison of the reflection and transmission parameters between the measured and simulated results for the two antennas without any isolation elements. The discrepancies between the curves can be primarily attributed to the circuit construction and the antenna connectors.

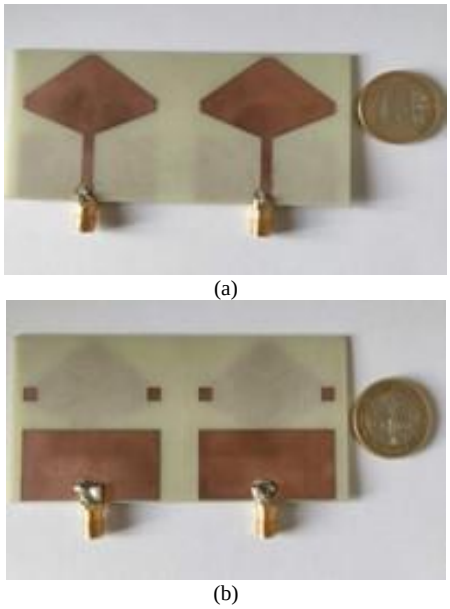

(a)

(b)

Fig. 16. Photos of the prototype antenna system: (a) in front view, (b) in back view.

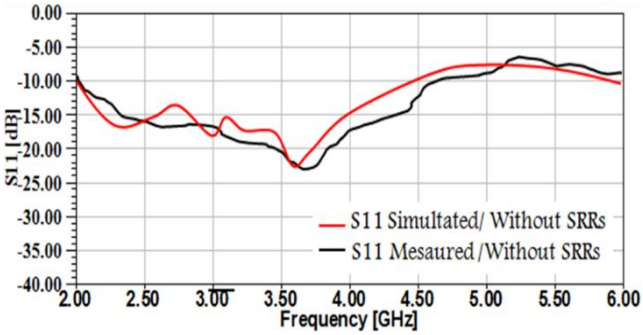

Fig. 17. Measured and simulated and S11 of the MIMO antenna.

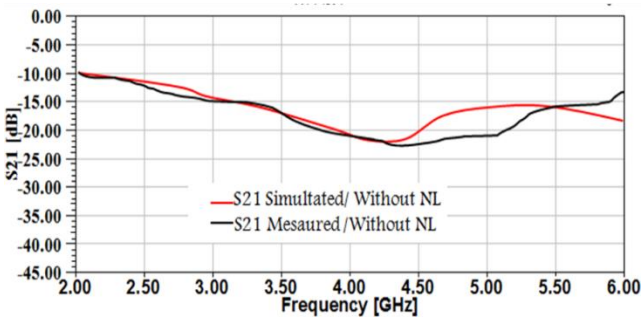

Fig. 18. Measured and simulated and S21 of the MIMO antenna.

IV. Reduction of Mutual Coupling Based on Neutralization Line and MTM

A. With NL

By positioning the antenna, you may keep some distance between them. We suggest a method to address the isolation issue, based on the placement of a neutralization line between the two antennas that were printed on the top surfaces of the FR-4 substrate (see Fig. 19).

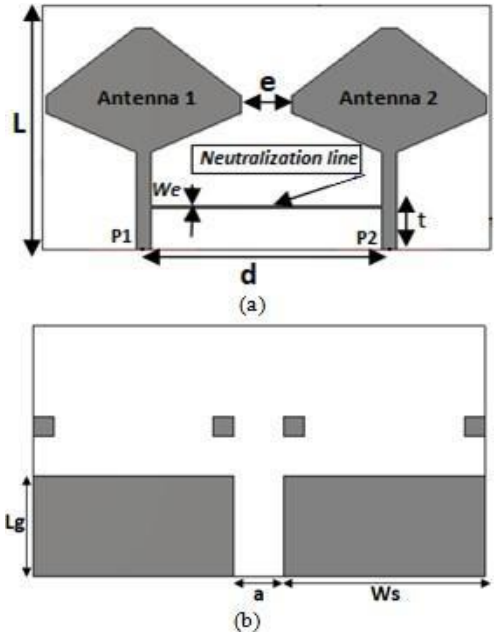

Fig. 19. Layout of a two-antenna MIMO system with NL: (a) front view, (b) bottom view.

To address the challenge of isolation while positioning the antennas with a certain degree of separation, we introduce an initial method. This method entails the insertion of a neutralization line positioned between the two antennas, printed onto the top surfaces of the FR-4 substrate, as depicted in Fig. 19. This technique is based on connecting the radiating elements to better decouple their power ports. In effect to make sure that the energy transmitted by one antenna is not wasted and radiated to the second antenna. Hence, it is important to reduce the parameter characterizing S21 which is taken as a parameter of the isolation between antenna ports. Indeed, the neutralization line was thin, short and will be taken as an inductance (see Table II).

TABLE I. PARAMETERS OF POSITION OF THE NEUTRALIZATION LINE

Parameters	Values (mm)
e	12.6
a	3.1
L	3.6
We	18.5
t	14

A parametric study on the position of the neutralization line in relation to the two supply ports is done to specify the efficiency of this line (NL). This study has been done with NL dimensions maintained at 45.5mm × 0.5mm. The reflection and transmission coefficients are illustrated in Fig. 20 and 21, respectively. In these two figures, the optimum position is t=9 mm, this value provides the high isolation at 3.5 GHz. Fig. 22 presents the transmission of radiation from antenna 1 to antenna 2 and the adaptation of antenna 1, in both situations of a MIMO system with and without NL. In simulation with a neutralization line, mutual coupling (S21) can be enhanced from -16 dB to more than -36 dB at 3.5 GHz. When the neutralization line was inserted, reflection coefficient was varied slightly. Fig. 23 shows that when antenna 1 is exited, there is less current in antenna 2 because all the current is concentrated on the neutralization line. So, the isolation in this case is enhanced.

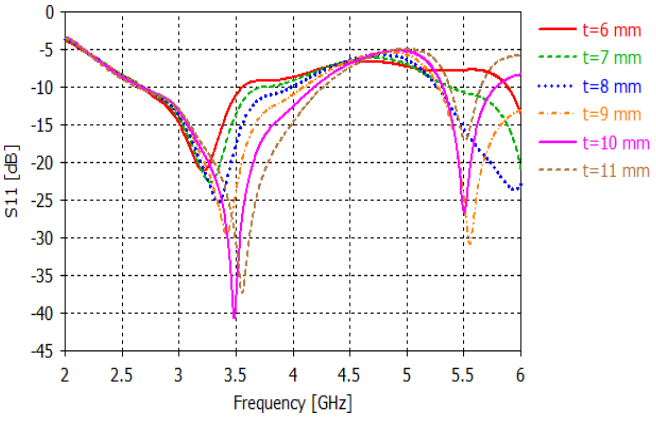

Fig. 20. Reflexion coefficient for different values of *t*.

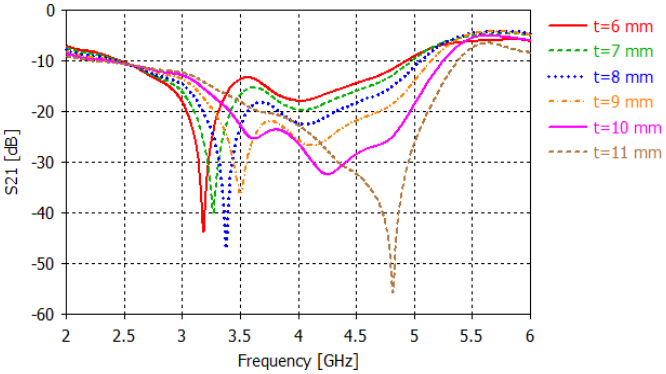

Fig. 21. Transmission coefficient for different values of *t*.

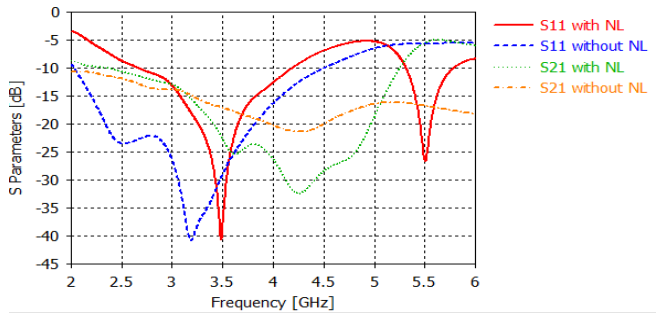

Fig. 22. Reflexion and transmission coefficients without and with NL.

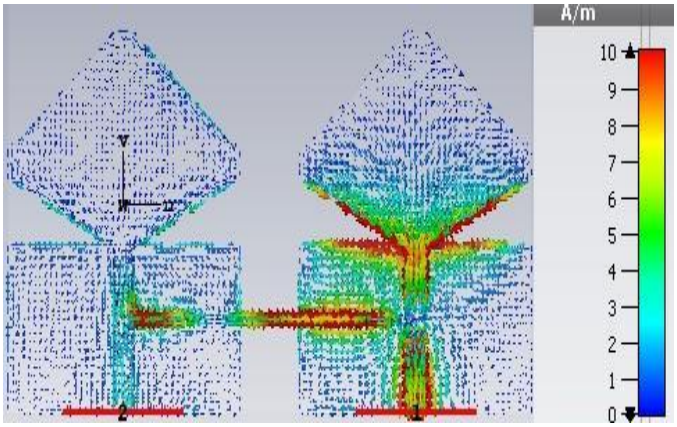

Fig. 23. Current distributions of the two antennas with NL at 3.5 GHz.

Theoretically, the NLs move some of the existing current from one antenna to the second antenna to remove the existing coupling. The envelope correlation coefficient (ECC) is an important factor to evaluate the capabilities of the MIMO/diversity antenna. ECC of the MIMO antenna system can be calculated using the radiation pattern or the S-parameters of the antenna. The envelope correlation can be expressed using the following expression:

$$ECC = \frac{|S_{11}^{*}S_{12}^{*} + S_{21}^{*}S_{22}^{*}|^2}{(1-|S_{11}|^2-|S_{21}|^2)(1-|S_{12}|^2-|S_{22}|^2)} \quad (1)$$

Another necessary parameter is its diversity gain (DG). It can be calculated with the following relation (2):

$$DG = 10\sqrt{1-(ECC)^2} \quad (2)$$

It is well that in desired band, the correlation envelope is very low (less than 0.2) as seen in Fig. 24. Also, we see that the gain is between 7 and 10 dB because the DG depends to a great part on the ECC and when ECC is minimal, DG is maximal as indicated in Fig. 25.

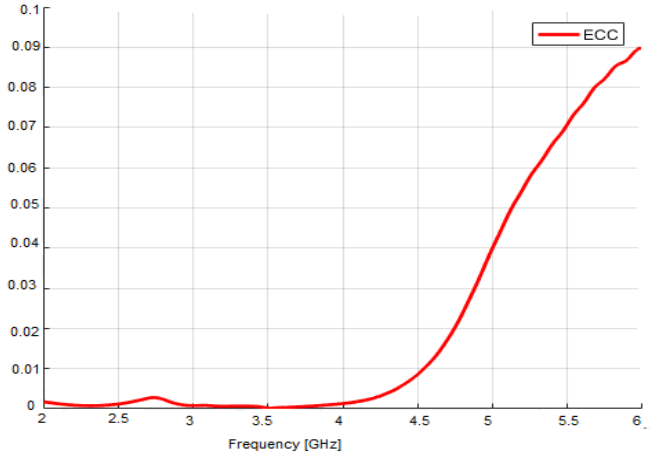

Fig. 24. ECC simulated for antenna 1 with NL.

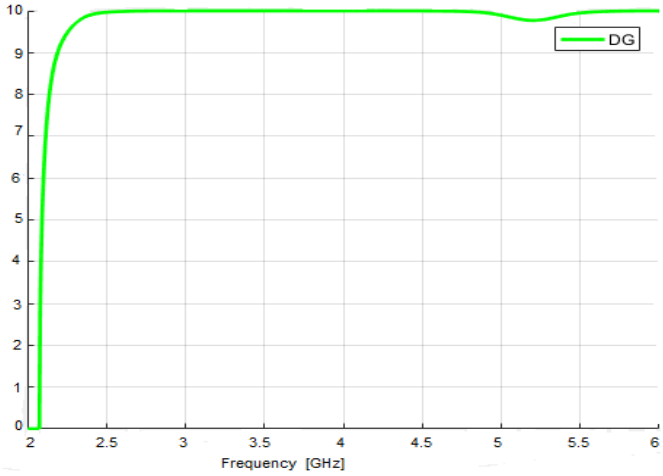

Fig. 25. DG simulated for antenna 1 with NL.

In Fig. 26, the radiation patterns of our investigated antenna are thoughtfully presented in both the horizontal (H) and vertical (E) planes. In this analysis, port 1 is excited while port 2 is loaded with 50 Ω impedance. This data showcases the antenna's remarkable unidirectional radiation pattern across both the E and H planes, consistently observed within the 3.5 GHz band. The tangible prototype of the two antennas integrated with the neutralization line (NL) is visually portrayed in Fig. 27, while Fig. 28 and 29 provide a direct comparison between the simulated and measured results of our antenna system. Notably, these figures illustrate the remarkable concordance between the two sets of data, further underscoring the efficacy of our antenna design. Furthermore, it's worth highlighting that the impedance bandwidth, defined by S11 < -10 dB, remains intact within the [3.4 - 3.8] GHz range, while S21 consistently maintains a level of less than -30 dB, affirming the antenna's outstanding performance in maintaining minimal mutual coupling.

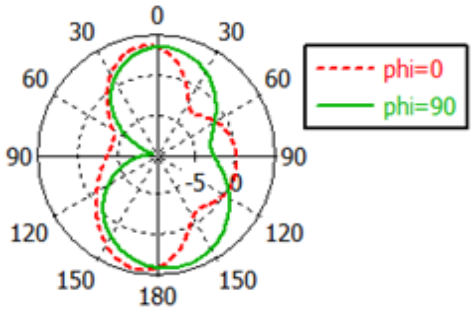

Fig. 26. Radiation patterns of antennas with NL in E and H planes at 3.5 GHz.

Fig. 27. Photos of the manufactured antenna system with NL technique.

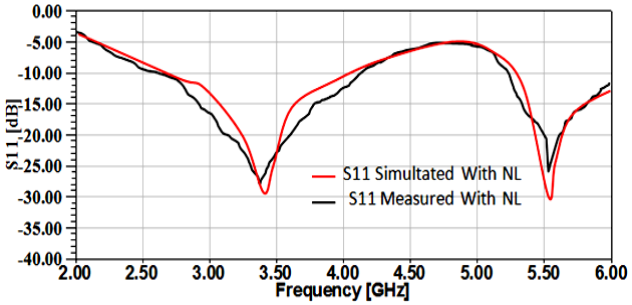

Fig. 28. Measured and simulated S11 of the MIMO antenna NL.

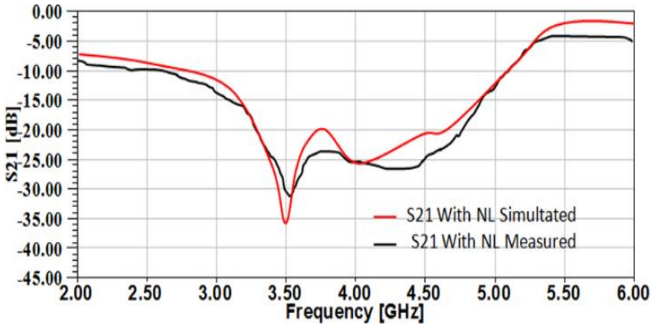

Fig. 29. Measured and simulated S21 of the MIMO antenna NL.

B. With MTM

Another technique to reduce the mutual coupling, we propose the insertion of a periodic array of SRR metamaterial composed of 3 cells. This technique will be implemented between two antenna elements with an edge-to-edge separation λ/8 (12.6 mm) at 3.5 GHz (Fig. 13). Fig. 30 presents the structure of the studied SRR, which is designed on a FR-4 dielectric substrate (thickness h = 1.6 mm, relative permittivity = 4.3).

SRRs possess the unique capability to manipulate electromagnetic fields, allowing us to create an environment that attenuates interference between antennas. By implementing SRRs, we establish an isolating structure that minimizes mutual coupling, which is essential for optimizing the performance and capacity of our MIMO system. In essence, SRRs act as a shield against interference, ensuring our antennas can function independently and efficiently, ultimately improving their overall performance.

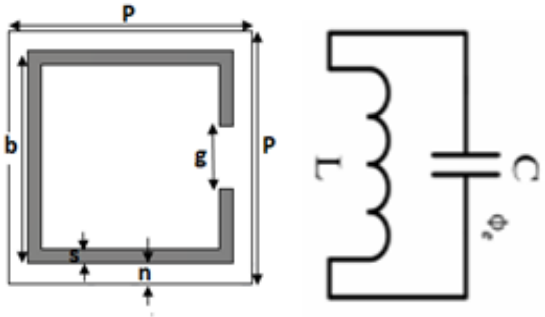

Fig. 30. Geometry of the SRR and his circuit equivalent model.

The resonance of the metamaterial can be characterized as an LC resonator and the resonant frequency is given by w=1/LC. The square-shaped SRR consists of a ring which represents the inductor effect and the gap is represented as the capacitor effect.

Fig. 31 shows the result of the simulation of the S parameters at the resonant frequency of 3.5 GHz. A reflection S11 around 0 dB with a transmission S21 tends towards -35 dB which confirms a phenomenon of stop band at 3.5 GHz of the metamaterial cell to ensure a better mutual decoupling in a cell network.

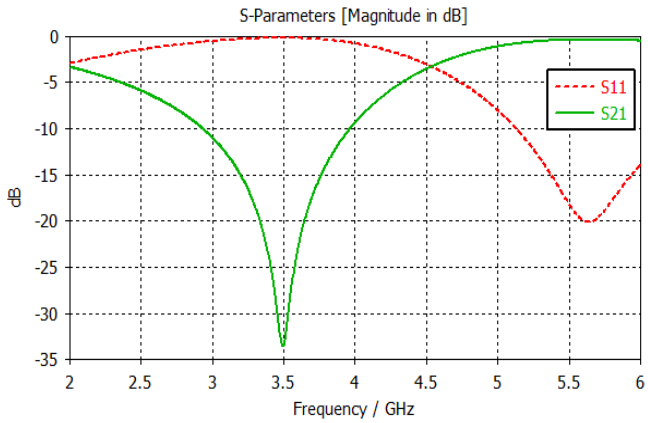

Fig. 31. Reflection and transmission coefficients of the SRR.

The square SRR under investigation has a side length P of 11 mm, with a 0.8 mm space (n) between the inner ring and the cell extremity, and a ring width (s) of 0.5 mm. When a perpendicular magnetic field is applied to the ring's plane, it begins to conduct, creating a current flow. This current enables the ring to function as an inductor, while the dielectric gap (n) generates a mutual capacitance. The resonant frequency of the SRR is determined by its dimensions, which are provided in Table III.

TABLE II. PARAMETERS OF SRR

Parameters	Values (mm)
p	12.6
b	8.9
s	0.5
n	0.8
g	3

The results of the simulation of S11 and S21 shown in Fig. 32 and 33, these results are in good accord in the whole [3.4 - 3.8] GHz band and illustrate that the cells of SRR act as a stop band (S11 = 0 dB and S21 <-10 dB).

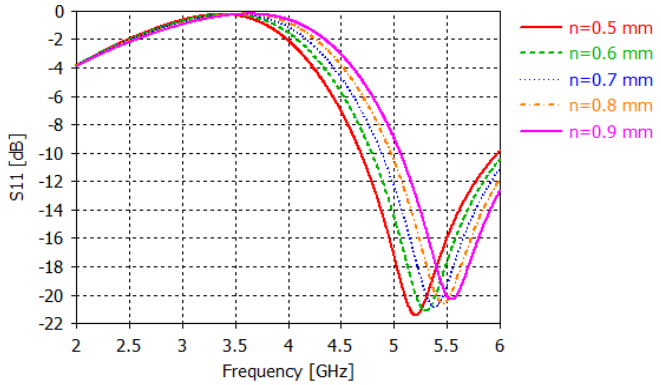

Fig. 32. S11 for a ran10ge of n-gap values.

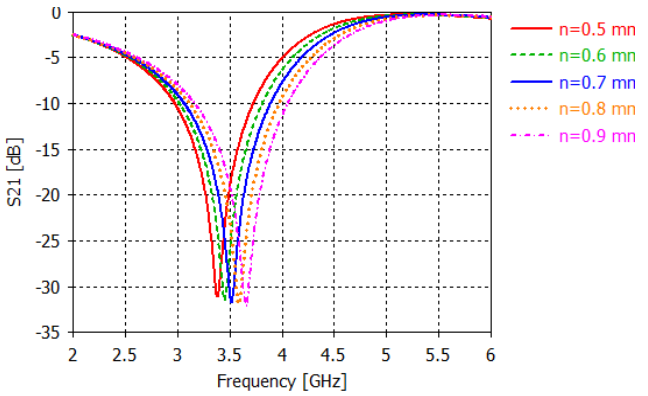

Fig. 33. S21 for a range of n-gap values.

In summary, the study demonstrates that the improvement in the n value is directly proportional to the increase in resonant frequency. To achieve the minimum value of S21, the chosen value for n is 0.8. After investigating the SRR, a new metamaterial structure consisting of a linear array of five identical SRR-type unit cells is placed between the two antennas to enhance the isolation at 3.5 GHz. The spacing between the two radiating elements' leading edges is set at 12.6 mm (Fig. 34). The dimensions and geometry of the studied SRR are provided earlier.

Fig. 35 shows that S11 remains below -10 dB throughout the 5G band, indicating good performance for the antenna both with and without the SRR. Moreover, the separation between the two antenna ports, P1 and P2, can be observed

from the S21 plot. By utilizing the SRR, the energy radiated from antenna 1 to antenna 2 is coupled at the SRR cell, resulting in improved isolation between the two antennas (S21 <-34 dB), as illustrated in Fig. 35. The parameter S21 is reduced by nearly 17 dB at 3.5 GHz, achieving good impedance matching for both antennas in the MIMO antenna system. Fig. 36 presents the current distribution of the MIMO antenna elements for both cases, with and without SRRs, when the P1 port is fed, and the P2 port is connected to a 50 Ω load. It can be observed that a portion of the current matches the SRR region, and the magnetic field is confined within the SRR region, leading to a decrease in mutual coupling between the antennas.

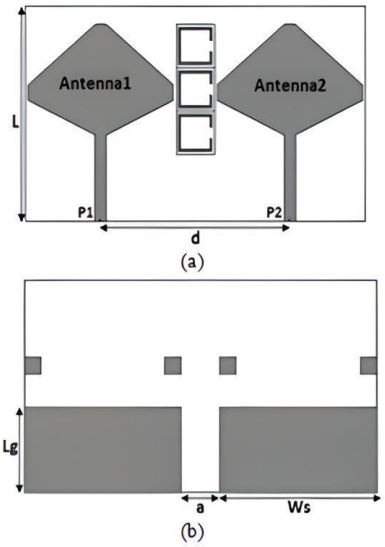

Fig. 34. Design of a two-antenna SRR MIMO system with SRRs: (a) in front view, in (b) bottom view.

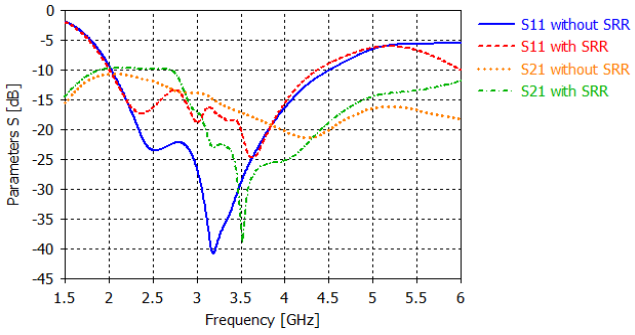

Fig. 35. Reflection and transmission coefficients without and with SRRs.

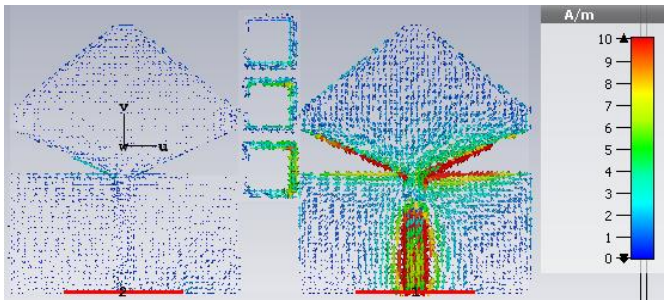

Fig. 36. Current distributions of the two antennas with SRRs at 3.5 GHz.

Fig. 37 and 38 provide crucial insights into the diversity gain (DG) of our antenna system. Notably, the diversity gain surpasses 9 dB, and its highest point aligns with the region where the correlation envelope is at its lowest. This observation underscores the significant impact of the envelope correlation coefficient (ECC) on diversity gain. A minimal correlation envelope signifies that the antennas are functioning independently and in an uncorrelated manner, which is instrumental for achieving higher diversity gain. In essence, the data in these figures emphasizes the pivotal role of ECC in influencing the diversity gain of our antenna system, highlighting the importance of ensuring low correlation between antennas for optimal performance.

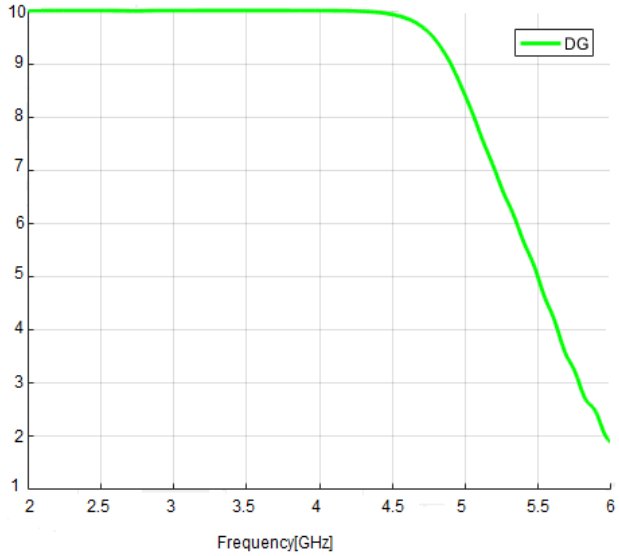

Fig. 37. DG simulated antenna 1 with SRRs.

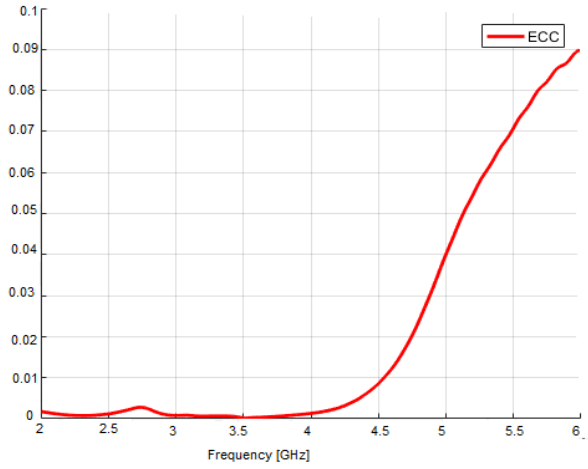

Fig. 38. ECC simulated for antenna 1 with SRRs.

Fig. 39 shows the radiation patterns of our MIMO antenna system in both cases with and without SRR. It is clearly seen that the radiation pattern is only affected by the SRR structure in the E and H planes. A prototype of the MIMO antenna described above has been manufactured and tested. Photos of the manufactured MIMO antenna are shown in Fig. 40.

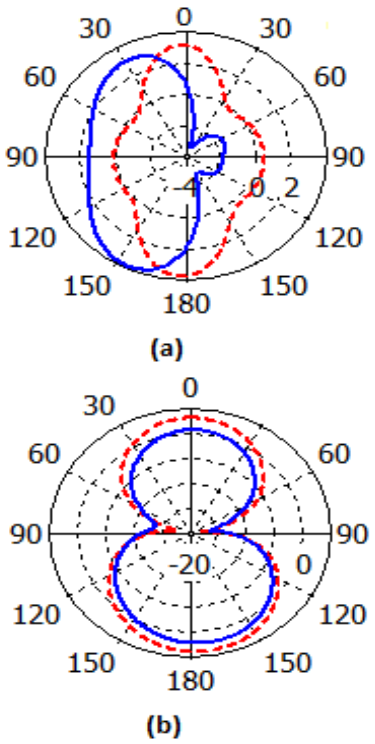

Fig. 39. Radiation patterns of antennas in both cases with and without SRR at frequency 3.5 GHz: (a) in E plane, (b) in H plane: dashed-line without SSR; solid-line with SRR.

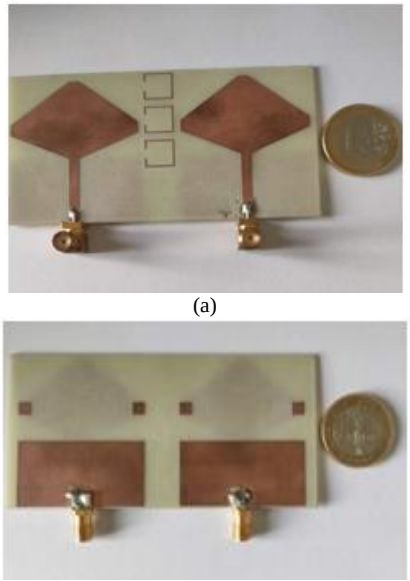

(a)

(b)

Fig. 40. Photos of the prototype antenna system with SRR technique: (a) in front view, (b) in back view.

The depicted Fig. 41 and 42 illustrate a comparison between the measured and simulated S parameters, specifically S11 and S21, for the MIMO antenna equipped with SRRs. These visual representations highlight a notable level of agreement, essentially validating our work. It's worth noting that any slight disparities observed between the two datasets can be largely attributed to factors like losses incurred by the measuring cable. Nonetheless, the overall congruence between the measured and simulated results reinforces the effectiveness of our antenna design and the reliability of our simulation, making a strong case for the practical viability of our approach.

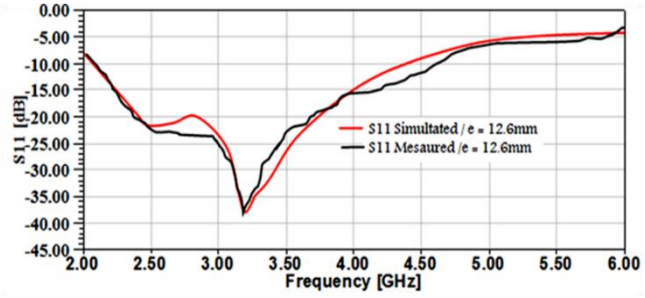

Fig. 41. Measured and simulated S11 of the MIMO antenna with SRRs.

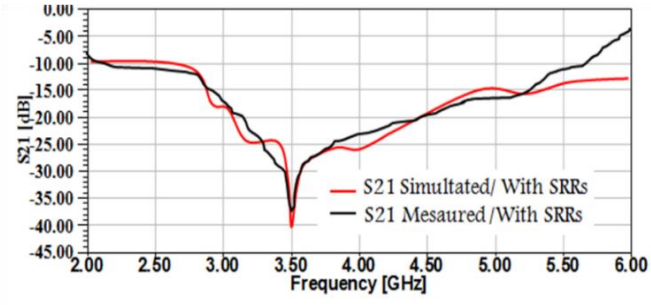

Fig. 42. Measured and simulated S21 of the MIMO antenna with SRRs.

V. Discussion and Results

The results presented in this study demonstrate the significant potential of the proposed techniques for enhancing the isolation characteristics of MIMO antennas operating in the 3.5 GHz frequency band, which is crucial for 5G and IoT applications. The use of a neutralization line (NL) and the integration of metamaterial split-ring resonators (SRRs) have shown remarkable improvements in reducing mutual coupling between adjacent antennas. The NL approach achieved an isolation of over 23 dB, while the SRR technique resulted in an isolation improvement of approximately 23 dB. These findings are particularly noteworthy when compared to existing methods in the literature. For instance, previous studies have reported lower isolation improvements, such as the 16 dB reduction achieved by a flag-shaped MIMO antenna using MTM technique and the 23 dB reduction with a circular antenna patch and MTM isolating structure. In contrast, our proposed techniques not only surpass these isolation levels but also maintain high gain and efficiency, as evidenced by the measured and simulated results. The gain of our antenna remained above 3.5 dB, and the efficiency reached above 80% in the working band with a frequency bandwidth of about 2.3 GHz. These results highlight the superior performance of our MIMO antenna design, making it a promising candidate for 5G and IoT applications. Furthermore, the practical implications of our findings are substantial. By improving the isolation characteristics of MIMO antennas, we can enhance the overall performance and reliability of 5G networks, enabling higher data rates, reduced interference, and better coverage. This is particularly beneficial for IoT applications,

where reliable and high-speed communication is essential for real-time monitoring and control of various devices and systems. Our findings provide valuable insights and practical solutions for the design of advanced MIMO antennas, contributing to the advancement of wireless communication technologies and the realization of the full potential of 5G and IoT. The effectiveness of the NL and SRR techniques is clearly demonstrated in Fig. 43 and 44, which show the reflection and transmission coefficients without and with the NL and SRRs, respectively. These figures illustrate the significant reduction in mutual coupling achieved by our proposed methods.

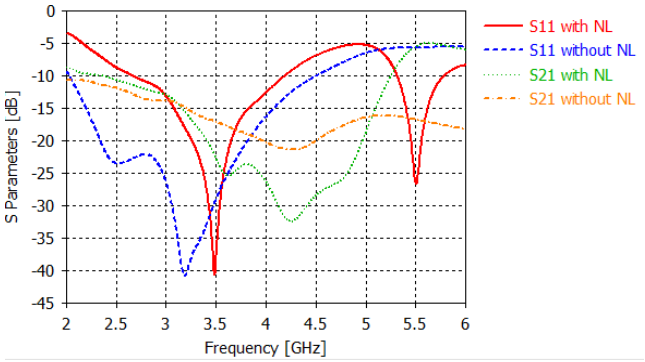

Fig. 43. Reflexion and transmission coefficients without and with NL.

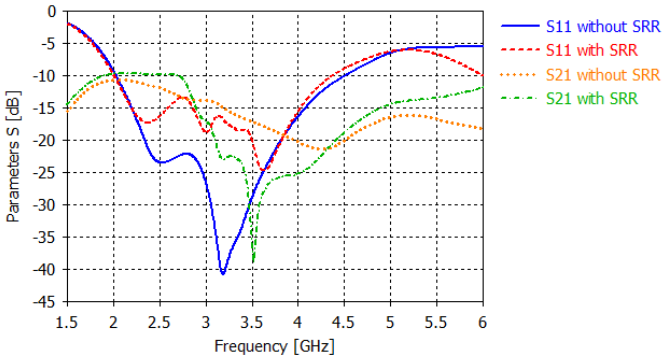

Fig. 44. Reflection and transmission coefficients without and with SRRs.

Table III presents a comparative analysis with other works in the field, highlighting the potential of our proposed techniques. This comparison underscores the advantages of our approach in terms of isolation enhancement, gain, and efficiency, demonstrating the superior performance of our MIMO antenna design for 5G and IoT applications.

TABLE III. TABLE OF COMPARISON WITH OTHER WORKS

Refs.	TECHNIQUE OF ISOLATION	EDGE-TO-EDGE GAP	MAX. ISOLATION IMPROVEMENT (dB)	GAIN (dB)	EFFICIENCY (%)
[27]	Metamaterial (MTM)	-	40	5.5	63
[28]	Metasurface (MTS)	0.26 ʎ	32	-	-
[29]	Slots	0.37 ʎ	26	4.4	-
THIS WORK	MTM/NL	0.12 ʎ	39/42	4.5	80

VI. CONCLUSION

In our paper, we have proposed a novel design of a system MIMO antenna array for 5G and IoT applications in the [3.4 - 3.8] GHz band of interest. We have described two techniques to present techniques for decreasing mutual coupling in antenna arrays applied to MIMO systems and a simulation of a MIMO antenna has been fully presented. These techniques are used to increase the isolation of our initially presented two-element system. The enhancement of the performance of our antenna system is obtained by using the neutralization line method to have isolation higher than 20 dB. On the other hand, with the method of insertion of the SRR periodic structures, the mutual coupling is minimized by about 23 dB. Simulation results show that the gain remains above 3.5 dB and the efficiency reaches above 80% in the working band with a frequency bandwidth about 2.3 GHz. Detailed parametric studies are done to find the right structure which is capable of responding to the demands of modern communication systems dedicated to 5G and IoT. Also, it is possible to apply the proposed neutralization line and the split ring resonator decoupling methods to design MIMO antennas with more than two radiation elements.

ACKNOWLEDGMENT

This research was funded by Taif University, Saudi Arabia, Project N° (TU- DSPP-2024-70).

REFERENCES

[1] Devi, Delshi Howsalya, Duraisamy, Kumutha, Armghan, Ammar, et al. 5g technology in healthcare and wearable devices: A review. Sensors, 2023, vol. 23, no 5, p. 2519.

[2] Khanh, Quy Vu, Hoai, Nam Vi, Manh, Linh Dao, et al. Wireless communication technologies for IoT in 5G: Vision, applications, and challenges. Wireless Communications and Mobile Computing, 2022, vol. 2022, no 1, p. 3229294.

[3] Huseien, Ghasan Fahim et Shah, Kwok Wei. A review on 5G technology for smart energy management and smart buildings in Singapore. Energy and AI, 2022, vol. 7, p. 100116.

[4] V. Avula, R. Nanditha, S. Dhuli, and P. Ranjan, "The Internet of Everything: A Survey," *2021 13th International Conference on Computational Intelligence and Communication Networks (CICN)*. IEEE, 2021. p. 72-79.

[5] Al-Malah, Duha Khalid Abdul-Rahman, Majeed, Ban Hassan, et Alrikabi, Haider Th Salim. Enhancement the educational technology by using 5G networks. International Journal of Emerging Technologies in Learning (Online), 2023, vol. 18, no 1, p. 137.

[6] Al-Gburi, Ahmed Jamal Abdullah, Zakaria, Zahriladha, Ibrahim, Imran Mohd, et al. Microstrip patch antenna arrays design for 5G wireless backhaul application at 3.5 GHz. In : Recent Advances in Electrical and Electronic Engineering and Computer Science: Selected articles from ICCEE 2021, Malaysia. Singapore : Springer Singapore, 2022. p. 77-88.

[7] Z. Davoody-Beni, N. Sheini-Shahvand, H. Shahinzadeh, M. Moazzami, M. Shaneh, and Gharehpetian, G. B, "Application of IoT in Smart Grid: Challenges and Solutions," In : *2019 5th Iranian Conference on Signal Processing and Intelligent Systems (ICSPIS)*. IEEE, 2019. p. 1-8.

[8] Anbarasu, Muthumanickam et Nithiyantham, Janakiraman. Performance analysis of highly efficient two-port MIMO antenna for 5G wearable applications. IETE Journal of Research, 2023, vol. 69, no 6, p. 3594-3603.

[9] Rafique Umair Khan, Suleman, Ahmed, Muhammad Mansoor, et al. Uni-planar MIMO antenna for sub-6 GHz 5G mobile phone applications. Applied Sciences, 2022, vol. 12, no 8, p. 3746.

[10] Surender, D., Khan, T., Talukdar, F. A., De, A., Antar, Y. M., and Freundorfer, A. P., "Key components of rectenna system: a comprehensive survey," *IETE Journal of Research*, 2020, p. 1-27.

[11] Lee, Young Seung, Jeon, Sang Bong, Pack, Jeong-Ki, et al. An In Vitro Experimental System for 5G 3.5 GHz Exposures. IEEE Access, 2022, vol. 10, p. 94832-94840.

[12] Z. Ren, A. Zhao, and S. Wu, "MIMO antenna with compact decoupled antenna pairs for 5G mobile terminals," *IEEE Antennas and Wireless Propagation Letters*, 2019, vol. 18, no 7, p. 1367-1371.

[13] Du, K., Wang, Y., & Hu, Y. (2022). Design and analysis on decoupling techniques for MIMO wireless systems in 5G applications. Applied Sciences, 12(8), 3816.

[14] Yang, C., Lu, K., & Leung, K. W. (2022). Dielectric decoupler for compact MIMO antenna systems. IEEE Transactions on Antennas and Propagation, 70(8), 6444-6454.

[15] Nadeem, I., and Choi, D. Y., "Study on mutual coupling reduction technique for MIMO antennas." *IEEE Access*, 2018, vol. 7, p. 563-586.

[16] Jiang, W., Liu, B., Cui, Y., and Hu, W., "High-isolation eight-element MIMO array for 5G smartphone applications," *IEEE Access*, 2019, vol. 7, p. 34104-34112.

[17] Zhou, W., Yue, C., and Li, Y., "Metamaterial Promoting 5G MIMO Antenna with Isolation Enhancement." In : *2021 International Applied Computational Electromagnetics Society (ACES-China) Symposium*. IEEE, 2021. p. 1-2.

[18] Daghari, M., Abdelhamid, C., Sakli, H., and Nafkha, K., "High Isolation with Neutralization Technique for 5G-MIMO Elliptical Multi-Antennas." In : *International conference on the Sciences of Electronics, Technologies of Information and Telecommunications*. Springer, Cham, 2018. p. 124-133.

[19] He, D., Yu, Y., and Mao, S., "Characteristic Mode Analysis of a MIMO Antenna with DGS." *2021 IEEE International Symposium on Antennas and Propagation and USNC-URSI Radio Science Meeting (APS/URSI)*. IEEE, 2021. p. 1143-1144.

[20] Alibakhshikenari, M., Vittori, M., Colangeli, S., Virdee, B. S., Andújar, A., Anguera, J., and Limiti, E. "EM isolation enhancement based on metamaterial concept in antenna array system to support full-duplex application." *2017 IEEE Asia Pacific Microwave Conference (APMC)*. IEEE, 2017. p. 740-742.

[21] Wan, L., Guo, Z., and Chen, X. (2019). "Enabling efficient 5G NR and 4G LTE coexistence." *IEEE Wireless Communications*, 2019, vol. 26, no 1, p. 6-8.

[22] Vaughan, R. G., and Andersen, J. B. "Antenna diversity in mobile communications." *IEEE Transactions on vehicular technology*, 1987, vol. 36, no 4, p. 149-172.

[23] Chen, J. H., Ye, L. H., Liu, T., & Wu, D. L. (2023). A low-profile dual-polarized patch antenna with simple feed and multiple decoupling techniques. IEEE Antennas and Wireless Propagation Letters, 22(8), 1883-1887.

[24] Alibakhshikenari, M., Virdee, B. S., See, C. H., Abd-Alhameed, R. A., Falcone, F., and Limiti, E. "Surface wave reduction in antenna arrays using metasurface inclusion for MIMO and SAR systems." *Radio Science*, 2019, vol. 54, no 11, p. 1067-1075.

[25] Megahed, A. A., Abdelazim, M., Abdelhay, E. H., and Soliman, H. Y. "Sub-6 GHz highly isolated wideband MIMO antenna arrays." *IEEE Access*, 2022, vol. 10, p. 19875-19889.

[26] Abd-Alhameed, R. A., and Limiti, E. "Mutual-coupling isolation using embedded metamaterial EM bandgap decoupling slab for densely packed array antennas." IEEE Access, 2019, vol. 7, p. 51827-51840.

[27] Supreeyatitikul, Nathapat, Phungasem, Anupan, et Aelmopas, Pongphol. Design of wideband sub-6 GHz 5G MIMO antenna with isolation enhancement using an MTM-inspired resonators. In : 2021 Joint International Conference on Digital Arts, Media and Technology with ECTI Northern Section Conference on Electrical, Electronics, Computer and Telecommunication Engineering. IEEE, 2021. p. 206-209.

[28] Sultan, Kamel S., Abdullah, Haythem H., Abdallah, Esmat A., et al. Metasurface-based dual polarized MIMO antenna for 5G smartphones using CMA. Ieee Access, 2020, vol. 8, p. 37250-37264.

[29] Sufian, Md Abu, Hussain, Niamat, Askari, Hussain, et al. Isolation enhancement of a metasurface-based MIMO antenna using slots and shorting pins. IEEE Access, 2021, vol. 9, p. 73533-73543.